MNRAS **000**, 1–9 (2024) Preprint 3 November 2024 Compiled using MNRAS LATEX style file v3.0

Testing the wavelength dependence of oscillations and granulation in red giants using *Kepler* and TESS

K. R. Sreenivas[1]★ ,Timothy R. Bedding[1], Daniel Huber[1,2], Courtney L. Crawford[1], Dennis Stello[3], May G. Pedersen[1], Yaguang Li[2], and Daniel Hey[2]
[1]*Sydney Institute for Astronomy, School of Physics, University of Sydney, NSW 2006, Australia.*
[2] *Institute for Astronomy, University of Hawai'i, 2680 Wood-lawn Drive, Honolulu, HI 96822, USA*
[3]*School of Physics, University of New South Wales, Sydney, NSW 2052, Australia.*

ABSTRACT
Stellar oscillations and granulation in red giants are both powered by convection. Therefore, studying the wavelength dependence of their amplitudes can provide useful insights on the driving mechanism. It is also important for plans to carry out asteroseismology with the Nancy Grace Roman Space Telescope, which operates in the near infrared, to check the dependence of oscillations and granulation on the observational wavelength. In this work, we aim to understand how the oscillation and granulation power in red giants depend on the wavelength and study how existing predictions compare with observations. We measure the mean oscillation and granulation power of 279 *Kepler* red giants, from the power density spectra derived using *Kepler* PDCSAP and TESS-SPOC light curves and compare their ratios. We find that selection of light curves is important for the study of amplitudes, as different light curve products show different values of amplitudes. We see that the oscillation and granulation power ratio between TESS and *Kepler* matches the theoretical prediction, suggesting that oscillation amplitudes decrease as we move to redder wavelengths. Further, we also see that the mean ratios of oscillations and granulation agree, suggesting that oscillation and granulation have the same wavelength dependence. We also find that the mean height-to-background ratio for *Kepler* agrees with previous results and show good agreement with TESS. These results suggest that the granulation signals would not severely affect the detection of oscillations. Also, the independence of power ratio between *Kepler* and TESS on stellar parameters suggest that the amplitudes of oscillation and granulation has same dependence on stellar parameters, in two different wavelength regimes.

Key words: red giants – stars: oscillations:red giants – stars: granulation

1 INTRODUCTION

Oscillations and granulation are two extensively studied phenomena in red giants. Oscillations are thought to be stochastically excited and damped by the convection in the outer layers (Goldreich & Keeley 1977a,b; Hekker & Christensen-Dalsgaard 2017; Houdek & Dupret 2015; Basu & Hekker 2020; Zhou et al. 2020). Analysis of the oscillation mode frequencies, amplitudes and linewidths help us to probe stellar interiors and retrieve global properties of stars (Chaplin & Miglio 2013; Jackiewicz 2021). Stellar granulation, a quasi-periodic intensity fluctuation predominant at low frequencies, is also thought to arise as a result of convection. The hot plasma from the outer convective zone rises to photosphere resulting in irregularly shaped bright cells (granules), which cools down to produce darker regions. This granulation produces brightness fluctuations whose power and time scale predominantly depends on the surface properties of the star (Trampedach et al. 1998; Ludwig et al. 2009; Mathur et al. 2011; Kjeldsen & Bedding 2011; Kallinger et al. 2014; Corsaro et al. 2017; Rodríguez Díaz et al. 2022).

With the large volume of observational data from CoROT and *Kepler* (Baglin et al. 2006; Jenkins et al. 2010), various efforts were made to check the validity of amplitude theories (Christensen-Dalsgaard & Frandsen 1983; Murray 1993; Samadi et al. 2012). While calculating the theoretical oscillation amplitudes, most of these studies assumed adiabatic nature for stellar oscillations and found discrepancies between calculated and observed amplitudes (Huber et al. 2011; Stello et al. 2011; Corsaro et al. 2013; Vrard et al. 2018). Although Samadi et al. (2012) accounted for the non-adiabatic effects, their study could not reproduce the observed amplitudes, only reduce the disagreement to 40 %. On the other hand, various studies have been done to investigate the dependence of granulation power on stellar parameters and are in agreement with

★ E-mail: skal9597@uni.sydney.edu.au

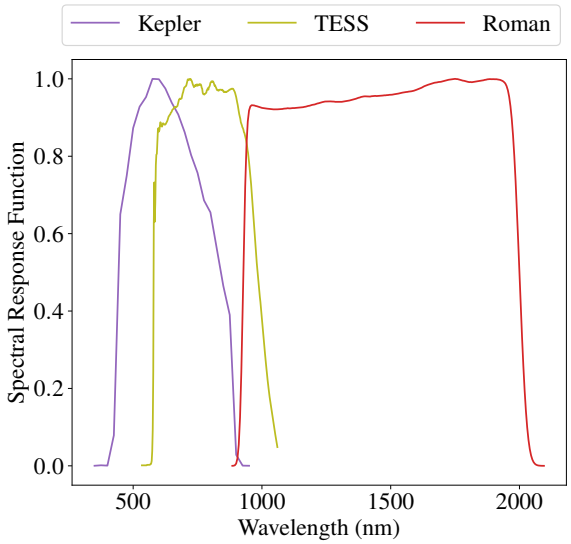

Figure 1. Spectral response function of *Kepler* (purple), TESS (light green) and Nancy Grace Roman Space Telescope (red).

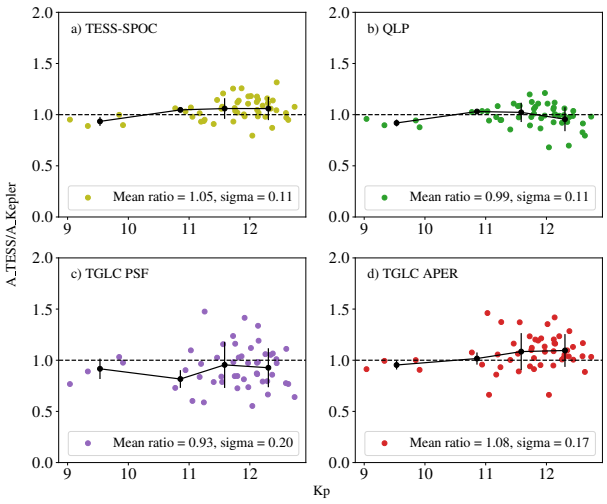

Figure 2. Ratio of amplitudes of 51 contact binaries in TESS relative to *Kepler* for various sources of light curves, as a function of *Kepler* magnitude. Panel a with TESS-SPOC light curves, panel b for QLP, panel c for TGLC PSF and panel d for TGLC APER light curves obtained from MAST. Error bars show the standard deviation in each bin.

each other (Mathur et al. 2011; Kallinger et al. 2014; Corsaro et al. 2017). All of these studies focused on studying the relationship between amplitudes and stellar parameters of solar-like oscillators.

By combining *Kepler* data with other space missions such as TESS (Transiting Exoplanet Survey Satellite) and Gaia (Ricker et al. 2014; Gaia Collaboration et al. 2016), it is possible to test predictions of how oscillation amplitudes and granulation power vary with wavelength (Aerts et al. 2010; Samadi et al. 2015). Kjeldsen & Bedding (1995) noted that the amplitude of oscillations decreases as we move to redder wavelengths. A systematic study by Lund (2019) showed that the amplitude of oscillation across the two pass bands varies with the ratio of their bolometric correction factor. Lund (2019) calculated bolometric correction factors through two separate methods: one by assuming a Planck spectrum and the other using synthetic stellar spectra. The ratio of oscillation amplitudes between *Kepler* and TESS was predicted to be around 0.83. Figure 1 shows the response curves of *Kepler*, TESS and Nancy Grace Roman Space Telescope (Van Cleve & Caldwell 2016; Ricker et al. 2014; Penny et al. 2019). As the wavelength coverage of TESS and Nancy Grace Roman Space Telescope is redder (fig. 1), we expect the oscillation amplitudes to be less than those observed in *Kepler*. Sulis, S. et al. (2020) showed that the oscillation and granulation levels for the Sun decreases as a function of wavelength, using VIRGO time series (Fröhlich et al. 1995).

Sulis, S. et al. (2023) studied two main sequence stars to compare their granulation amplitudes, obtained from contemporaneous radial velocity and photometric observations. The granulation amplitudes from their ESPRESSO (Pepe et al. 2013) and CHEOPS (Benz et al. 2021) observations matched the predictions made by 3D hydro-dynamical models. However, such an agreement could not be established with TESS photometry due to large white noise. Further, in red giants it has been observed that the region of oscillations in the frequency domain contain some level of granulation signal, hence is often considered as noise (Huber et al. 2009; Mosser et al. 2012; Mathur et al. 2011). Therefore, a proper analysis regarding the behaviour of oscillation and granulation among different stellar types is relevant to understand the wavelength sensitivity and thus formulate mitigation strategies.

In this paper, we focus on how the observed oscillation and granulation amplitude ratios compares with prediction for a large number of stars, for *Kepler* and TESS. With upcoming launch of the Nancy Grace Roman Space Telescope, which will measure oscillations in red giants in the near infrared (Gould et al. 2015; Huber 2020), it is important check whether the observations align with the theoretical predictions.

2 DATA, TARGET SELECTION AND METHODOLOGY

2.1 Light curves

We used the Long Cadence (29.4 min) light curves from the *Kepler* mission, processed through the PDCSAP algorithm from the SPOC (Stumpe et al. 2012; Smith et al. 2012), spanning over 1200 days. From TESS, we used the TESS-SPOC light curves derived from Full-Frame Images (FFIs) using the SPOC algorithm (TESS-SPOC, Jenkins et al. 2016; Caldwell et al. 2020). Note that we did not apply any additional filtering to the light curves.

2.1.1 Tests using contact binaries

SPOC is one of several pipelines that have been used to create light curves from TESS data. Each pipeline selects the aperture used for extracting the light curve in different ways. Also, correction for systematic effects, such as background light, is carried out differently, which could affect the measurement of the amplitudes. Therefore, in order to check the amplitudes measured by TESS-SPOC, we examined a sample of contact binaries. Contact binaries show near sinusoidal variations in their light curve, whose periods are accurately determined (Prša et al. 2011). These variations are due to tidal distortion, hence should have similar amplitudes when observed through the *Kepler* and TESS band passes. To check whether the extraction of light from FFI's and de-trending method influences

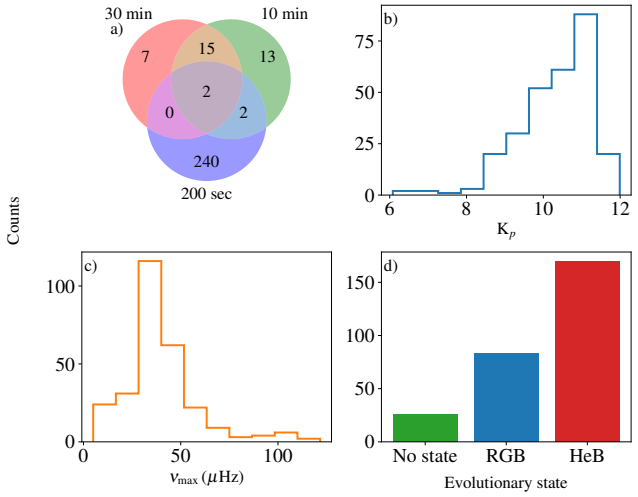

Figure 3. Distribution of various parameters for the stars in our list. Panel a shows the distribution of TESS-SPOC data for the targets used in this study. Panel b shows the distribution of *Kepler* magnitude, panel c shows the distribution of $\nu_{\rm max}$ in μHz from Yu et al. (2018) and panel d shows the distribution of evolutionary states from Yu et al. (2018).

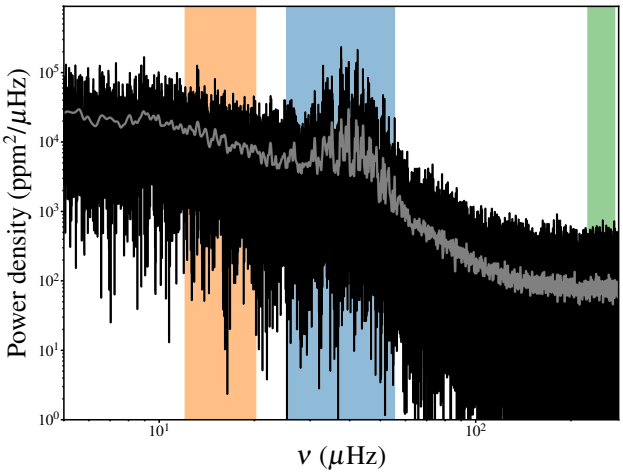

Figure 4. Power density spectrum from *Kepler* light curve of a typical red giant star. The grey curve is the smoothed power spectrum. The orange region is region 1, blue for region 2 and region 3 is in green.

the amplitudes, we also examined the TESS light curves processed using QLP pipeline (Quick Look Pipeline; Huang et al. 2020a,b) and the TGLC pipeline (TESS–Gaia Light Curve), which uses Gaia catalog as a prior to derive the light curve (Han & Brandt 2023). Since the TGLC data products for *Kepler* stars are available only for sector 14 and 15, we only used these two sectors of data from all the above light curve products. In addition, we ensured that all time series have the same time span of observations as TESS-SPOC.

We selected 51 contact binaries from Prša et al. (2011) that have TESS-SPOC, QLP and TGLC light curves. For each star, we calculated the amplitude spectrum of the light curve from each of the pipelines. We measured the amplitude of the highest peak from *Kepler* and then measure the amplitudes, at the same frequency in each of the TESS light curves. It should be noted that the highest peak was at half of the reported period of binary orbit because the two components have very similar tidal distortions.

Figure 2 shows the ratio of amplitudes of TESS to *Kepler* at the measured frequency, as a function of *Kepler* magnitude. It can be seen that the TESS pipelines show reasonable agreement with amplitudes from *Kepler*. The amplitude ratios from the SPOC-generated light curves have similar scatter to those from QLP light curves and the scatter from TGLC is greater. This test confirms that TESS-SPOC light curves are suitable for this project. Moreover, a scatter of 11 % on the ratios can be viewed as a minimum scatter to be expected when comparing oscillation and granulation ratios, in addition to the variability due to the stochastic nature of oscillation and granulation.

2.2 Sample selection

The asteroseismic characteristics of *Kepler* red giants have been thoroughly examined (Huber et al. 2011; Mosser et al. 2012; Kallinger et al. 2014; Yu et al. 2018). These catalogues mainly contain estimates of the frequency of maximum power ($\nu_{\rm max}$, Brown et al. 1991; Kjeldsen & Bedding 1995) and the large frequency separation ($\Delta\nu$; Tassoul 1980), determined by analysing frequency spectra using dedicated pipelines (Hekker, S. et al. 2012; Mathur et al. 2011).

Stello et al. (2022) carried out a magnitude limited analysis of 16000 *Kepler* red giants from Yu et al. (2018), using two sectors of TESS light curves. This resulted in a subset of stars which show clear power excess with TESS, at the previously reported *Kepler* $\nu_{\rm max}$. They measured $\nu_{\rm max}$ values for 2724 stars and $\Delta\nu$ values for 570 stars from the TESS data, using the SYD pipeline (Huber et al. 2009). Here we used the 223 Kepler red giants from Stello et al. (2022) that have at least one sector of TESS-SPOC data. We also included 48 Kepler red giants from Yu et al. (2018) that are not present in Stello et al. (2022), but which show clear oscillations in TESS-SPOC.

Figure 3 shows the distribution of parameters for the 279 stars in our list. From panel a, most of the stars (about 90 %) in our study are from the second extended mission of the TESS, with FFI light curves having a cadence of 200 s. Note that, 256 stars in this sample have only one sector of TESS data. Panel b shows the distribution of the *Kepler* magnitude of the stars. We restrict ourselves to stars with *Kepler* magnitudes less than 12. From Fig. 3 c, it can be seen that most stars in our sample have $\nu_{\rm max}$ values $\sim$ 30 to 70 μHz and none are above 124 μHz. This is because of two reasons: the non-availability of TESS-SPOC light curves for a larger sample and the inability of TESS to detect oscillations at higher $\nu_{\rm max}$ with short datasets (Hon et al. 2021; Stello et al. 2022). Fig 3 d shows the evolutionary state of the red giants in our sample, and about 70 % of the stars burn Helium in their core (HeB).

2.3 Methodology

Since our aim is to compare oscillations and granulation of the same star observed with *Kepler* and TESS, which have different time spans and cadences, it is important that we do our analysis in power density. Analysis in power density units ensure that the measured quantities are independent of the time span of observations (Kjeldsen & Bedding 1995; Kjeldsen et al. 2005). For *Kepler*, we calculated the power density spectra of the full light curves up to the Nyquist frequency (283 μHz). For TESS data, because the observational cadence was sometimes different between sectors, we

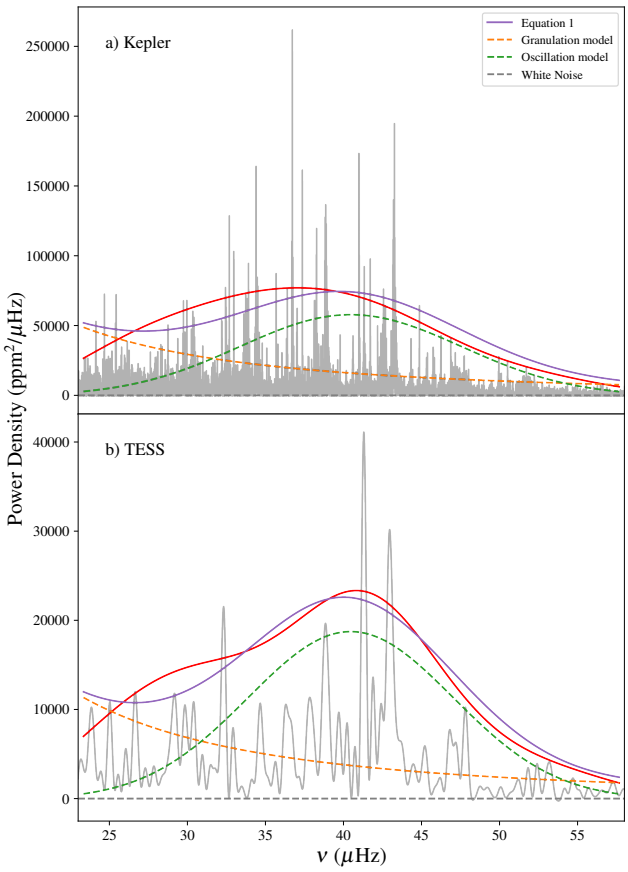

Figure 5. Fit to the power density spectrum to determine the oscillation and granulation amplitudes. The top panel shows the fit to the power density spectrum from *Kepler* and bottom panel shows the same for TESS. The red line shows the smoothed power density spectrum on which eq. 1 is fitted (purple line). The orange and green dashed line shows the background component and oscillation component, respectively. The grey dashed line corresponds to the white noise, kept constant during the fitting.

first constructed the power spectra (in ppm^2) of each sector (Lomb 1976; Scargle 1982; Press & Rybicki 1989), up to the lowest Nyquist frequency ($\nu_{\rm Nyq}$) among all sectors. These were converted to power density (in ppm^2/μHz) by multiplying by the effective observation time, which is the number of points multiplied by the cadence of each sector.

The averaging of signal during each data point causes the attenuation of amplitudes (Huber et al. 2009; Chaplin et al. 2011; Kallinger et al. 2014). Correction for this is important since we are comparing amplitudes from *Kepler* and TESS, where the exposure times are different. To correct for this, we first calculated the high frequency noise from $0.8\nu_{\rm Nyq}$ to $0.97\nu_{\rm Nyq}$. We subtracted this high frequency noise from power density spectra and divided by sinc$^2\left(\frac{\pi}{2}\frac{\nu}{\nu_{\rm Nyq}}\right)$. We then averaged power density spectra from individual sectors, resulting in the final power density spectra of the star.

2.3.1 *Method 1: Using Mean powers*

Since solar-like oscillators are stochastic, the oscillation power at any point of time would be fluctuating about the mean power. In order to measure the oscillation and granulation power, we first employed a simple and uniform approach. We used the $\nu_{\rm max}$ values from Sreenivas et al. (2024) to anchor the regions where the oscillation and granulation are prominent. We define 3 regions of interest in the power density spectrum of a star (Fig. 4), region 1 for granulation (orange), region 2 for oscillations (blue) and region 3 (in green) for measuring white noise.

Firstly, the white noise was measured in region 3, from $0.8\nu_{\rm Nyq}$ to $0.97\nu_{\rm Nyq}$. Previous studies have shown that the power becomes purely granulation in nature between 800 μHz to 1000 μHz for the Sun (Karoff et al. 2013 and references therein), which spans from 0.26 to 0.32 times $\nu_{\rm max\odot}$. Because of the shorter time span of TESS data and to get accurate measurements, we define a slightly wider granulation region compared to the main-sequence case, from $0.3^*\nu_{\rm max}$ to $0.5^*\nu_{\rm max}$ and the mean power in this region is used for granulation, termed as $\langle P_{\rm gran}\rangle$. This choice ensures that power measured is free of long term stellar signals at lower frequencies and is purely due to stellar granulation.

We measured the mean oscillation power, $\langle P_{\rm osc}\rangle$, in region 2, with boundaries from $\nu_{\rm max} - \delta\nu_{\rm env}$ to $\nu_{\rm max} + \delta\nu_{\rm env}$. We set $\delta\nu_{\rm env}$ to equal the approximate value of the full-width at half-maximum (FWHM) of the power excess envelope, which can be estimated from its power law relation with $\nu_{\rm max}$ (Mosser et al. 2012; Stello et al. 2022). To find the coefficients in this power law, we fitted the FWHM values measured by Yu et al. (2018), using their uncertainties as weights in the fit and only including stars for which the FWHM was measured to better than 10%. The resulting fit gave the FWHM as $0.78(\nu_{\rm max}/\mu{\rm Hz})^{0.80}$. It should be noted that region 2 also includes a contribution from granulation, but still gives a good measure of oscillation power.

2.3.2 *Method 2: Modelling the power excess*

Although the method described in Sec. 2.3.1 is straightforward, it does not account for granulation power in the region of oscillations. Since we are focused on the region of power excess, we determined the granulation power at $\nu_{\rm max}$ ($B_{\nu_{\rm max}}$) and oscillation power ($H_{\rm osc}$) using the fitting procedure in a local region of oscillations (Mosser et al. 2012; Gehan et al. 2023). We first smoothed the power density spectrum using a Gaussian kernel with a width of $2\Delta\nu$. In order to isolate the power excess, we fitted to a region $[\nu_{\rm max} - \delta\nu_{\rm env}, \nu_{\rm max} + \delta\nu_{\rm env}]$. We fitted the following equation to this smoothed spectrum:

$$P(\nu) = B_{\nu_{\rm max}}\left(\frac{\nu}{\nu_{\rm max}}\right)^{\alpha} + H_{\rm osc}\exp\left(\frac{-(\nu-\nu_{\rm max})^2}{2\sigma^2}\right) + W \qquad (1)$$

Here, α is the exponent that controls the shape of the background and we choose to fix α = -2 (following Mathur et al. 2011; Mosser et al. 2012; Kallinger et al. 2014; Sreenivas et al. 2024). σ is the standard deviation of the oscillation envelope, which is $\delta\nu_{\rm env}$/2.35; $H_{\rm osc}$ is the power density at $\nu_{\rm max}$. W is the constant high frequency noise in the power density spectra, which is measured as per section 2.3.1 and is kept constant at this value throughout the fitting process. Figure 5 shows the fit to the power density spectrum of a red giant, using *Kepler* data (panel a) and TESS data (panel b).

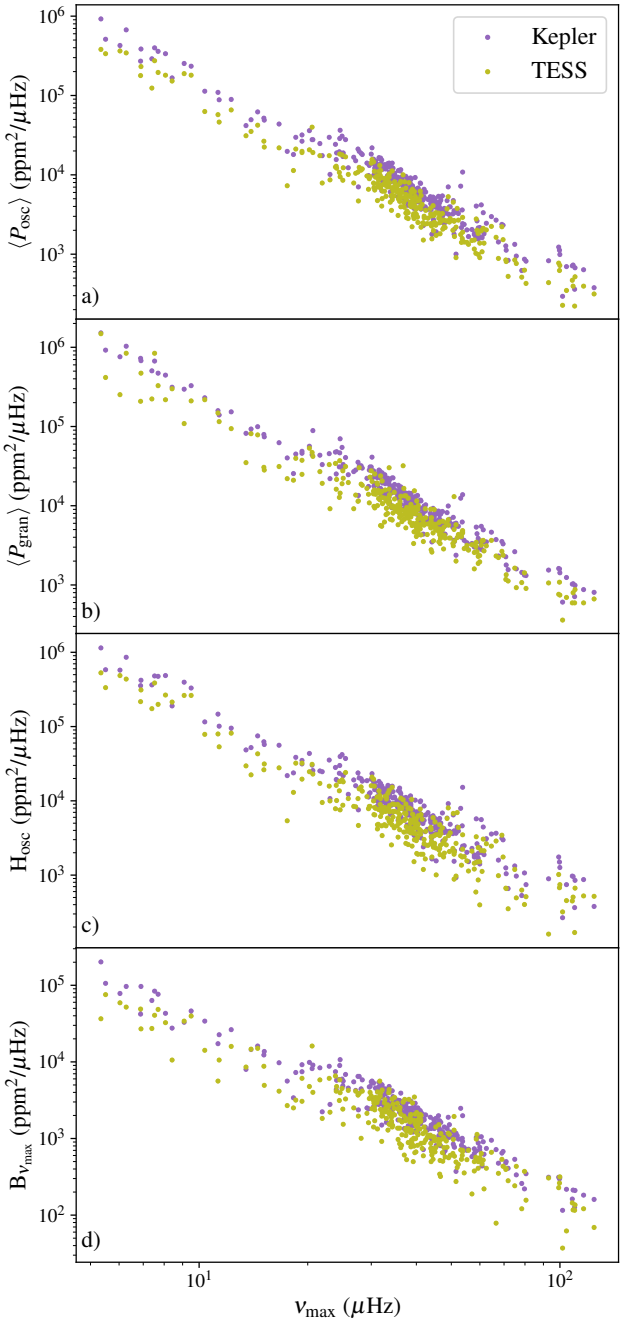

Figure 6. Oscillation and granulation powers determined using the two methods from this work, for *Kepler* (purple) and TESS (light green) data. $\langle P_{osc} \rangle$ in panel a, $\langle P_{gran} \rangle$ in panel b, H_{osc} in panel c, and $B_{\nu_{max}}$ in panel d

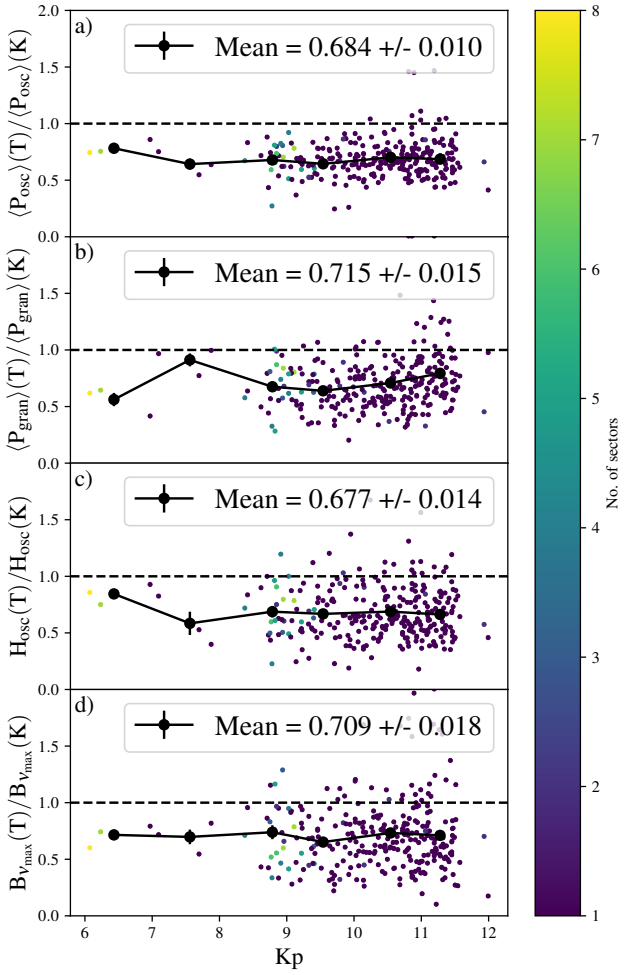

Figure 7. Ratios of oscillation power in TESS to *Kepler* (panel a and b) Ratios of granulation power in TESS to *Kepler* (panel c and d), plotted as a function of *Kepler* Magnitude for red giants, color-coded with number of sectors in TESS-SPOC data. Panel a shows the ratio of mean oscillation power ($\langle P_{osc} \rangle$) in TESS to *Kepler* and Panel b shows ratio of mean oscillation power ($\langle P_{gran} \rangle$) in TESS to *Kepler*. Panel c and d shows the ratio of H_{osc} and $B_{\nu_{max}}$ between TESS and *Kepler*, respectively.

3 RESULTS AND ANALYSIS

3.1 Validating the oscillation and granulation parameters

Figure 6 shows the oscillation power ($\langle P_{osc} \rangle$ and H_{osc}) and granulation powers ($\langle P_{gran} \rangle$ and $B_{\nu_{max}}$) as a function of ν_{max}, from *Kepler* (in purple) and TESS data (light green).We fitted a polynomial of the form $a{\nu_{max}}^b$ to these powers, and the results are shown in Table 1. The $\langle P_{osc} \rangle$ value does not represent an exact measurement of oscillation, as we do not remove the granulation power by modelling, while the H_{osc} from fitting is a more accurate measure of

Mission	parameter	a	b
Kepler	$\langle P_{osc} \rangle$	0.57±0.06	−2.36±0.04
	$\langle P_{gran} \rangle$	0.81±0.05	−2.37±0.03
	H_{osc}	0.70±0.07	−2.42±0.04
	$B_{\nu_{max}}$	0.70±0.06	−2.14±0.04
TESS	$\langle P_{osc} \rangle$	0.30±0.06	−2.30±0.04
	$\langle P_{gran} \rangle$	0.49±0.06	−2.28±0.04
	H_{osc}	0.42±0.08	−2.36±0.05
	$B_{\nu_{max}}$	0.42±0.08	−2.08±0.05

Table 1. Table of fitted parameters, when a model of the form $a{\nu_{max}}^{\beta}$ was fitted to oscillation and granulation powers.

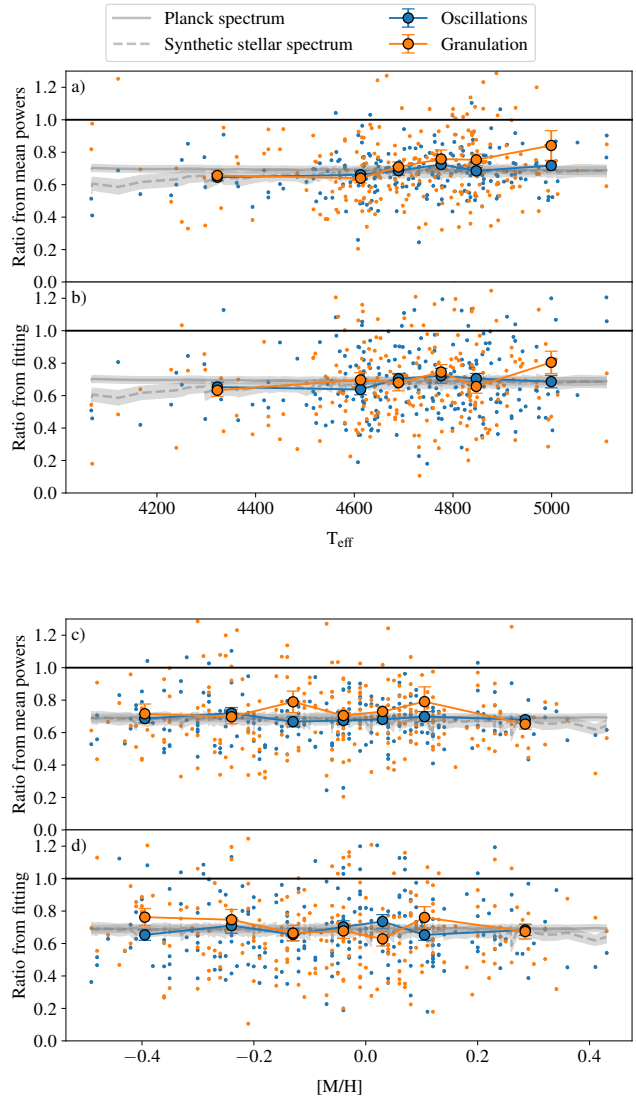

Figure 8. Variation in ratio as function of stellar parameters. Blue circles represent the ratio of oscillation power in TESS to *Kepler*, and orange represent the same for granulation. Panel a shows the ratios of mean power (method 1) as a function of effective temperature and Panel b shows the same from fitted parameters (method 2). Panels c and d shows the same ratios, as a function of metallicity. Larger circles show the mean in each bin, and error bars show the SEM. The solid and dashed grey lines represent the predictions from Lund (2019) based on Planck spectrum and stellar synthetic spectra, respectively. The grey region around these lines show the error bars for the predicted ratios.

oscillations. The value of b for the $H_{\rm osc}$ fits (-2.42 for *Kepler* and -2.36 for TESS) are closer to the exponents listed in Mosser et al. (2012), which were based on the first 590 days of *Kepler* data.

Panel b of Fig. 6 shows the correlation of $\langle P_{\rm gran}\rangle$ with $\nu_{\rm max}$. We find that $\langle P_{\rm gran}\rangle \propto {\nu_{\rm max}}^{-2.37}$ for *Kepler* and $\langle P_{\rm gran}\rangle \propto {\nu_{\rm max}}^{-2.28}$ for TESS, confirming the relation between $\nu_{\rm max}$ and granulation power from previous studies (Mathur et al. 2011; Mosser et al. 2012). The $B_{\nu_{\rm max}}$ values also show this correlation with $\nu_{\rm max}$, $B_{\nu_{\rm max}} \propto {\nu_{\rm max}}^{-2.08}$.

3.2 Ratios between TESS and *Kepler*

3.2.1 *Dependence on observational parameters*

We now compare the oscillation and granulation powers of stars in our sample. Figure 7 shows the ratio of TESS to *Kepler* for oscillation and granulation power, as a function of *Kepler* magnitude. The individual stars are color coded with the number of sector of TESS data and no correlations can be seen. In general, we could not see any significant trend in these ratios as a function of brightness, giving confidence that the white noise is being correctly subtracted. The scatter of ratios is similar at all brightness levels, suggesting that this scatter does not arise from photon noise and instead arises from the stochastic nature of the processes that excite and damp the oscillations and granulation.

Fig. 7a shows the ratio of mean oscillation power $\langle P_{\rm osc}\rangle$ (in ppm$^2/\mu$Hz) between *Kepler* and TESS, measured using method 1 (see Sec 2.3.1). We tested whether the choice of boundaries have any effect on the results by changing the boundaries of these regions used to measure mean power. We changed these boundaries by 20 % and found that the ratios in each case agree each other within the Standard Error on the Mean (SEM). Fig. 7c shows the ratios of $H_{\rm osc}$ values, which are obtained from fitting (method 2). The mean ratios from two methods agree, which is consistent with the fact that the exponents of the power law fit to $\langle P_{\rm osc}\rangle$ and $H_{\rm osc}$ are very similar for these two, both in *Kepler* and TESS. The predicted value of oscillation power ratio between TESS and *Kepler* is ~ 0.69 (Lund 2019). We see a mean value of 0.68 ± 0.01 for the $\langle P_{\rm osc}\rangle$ ratio and 0.68 ± 0.01 for the $H_{\rm osc}$ ratio, is excellent agreement with theoretical expectations.

Similarly, Fig 7 b and d shows the ratio of granulation power between TESS and *Kepler*, measured using both methods. The mean ratio of $\langle P_{\rm gran}\rangle$ TESS to *Kepler* is found to be 0.72 ± 0.02 (panel b) and the mean ratio of $B_{\nu_{\rm max}}$ is 0.71 ± 0.02. Most importantly, the results confirm that oscillation and granulation has the similar wavelength dependence. On comparing $H_{\rm osc}$ (panel c) and $B_{\nu_{\rm max}}$ (panel d), it is evident that the granulation power at $\nu_{\rm max}$ behaves similar to granulation power at low frequencies, in any wavelengths.

For the 7 % of stars in our sample that have multiple sectors with gaps, it is interesting to check whether the window function influences these ratios. For this, we also computed the ratios with only the first available sector of each star, and found that they are in good agreement (within 1 SEM) with the values of ratios obtained from full light curve. We also checked how these ratios depend on observational length of both TESS or *Kepler*. For this, we cut out a segment from *Kepler* time series having same time span as effective observation time of TESS. We then followed the same methods as before, to calculate the oscillation and granulation powers. Again the mean ratios between *Kepler* and TESS were the same within uncertainties.

3.2.2 *Dependence on stellar parameters*

Our measurements allow us to check whether the ratios between in two pass-bands depend on stellar parameters. The theoretical study by Lund (2019) suggest that the oscillation ratio depends on effective temperature and metallicity, with logg having little effect. For this analysis, we used the effective temperatures and metallicities from Yu et al. (2023), which contains stellar parameters for the 229 stars in our sample. Figure 8 shows the different ratios as a function of effective temperature (panels a and b) and metallicity (panels c and d). We do not see any dependence of the ratios on any of these parameters.

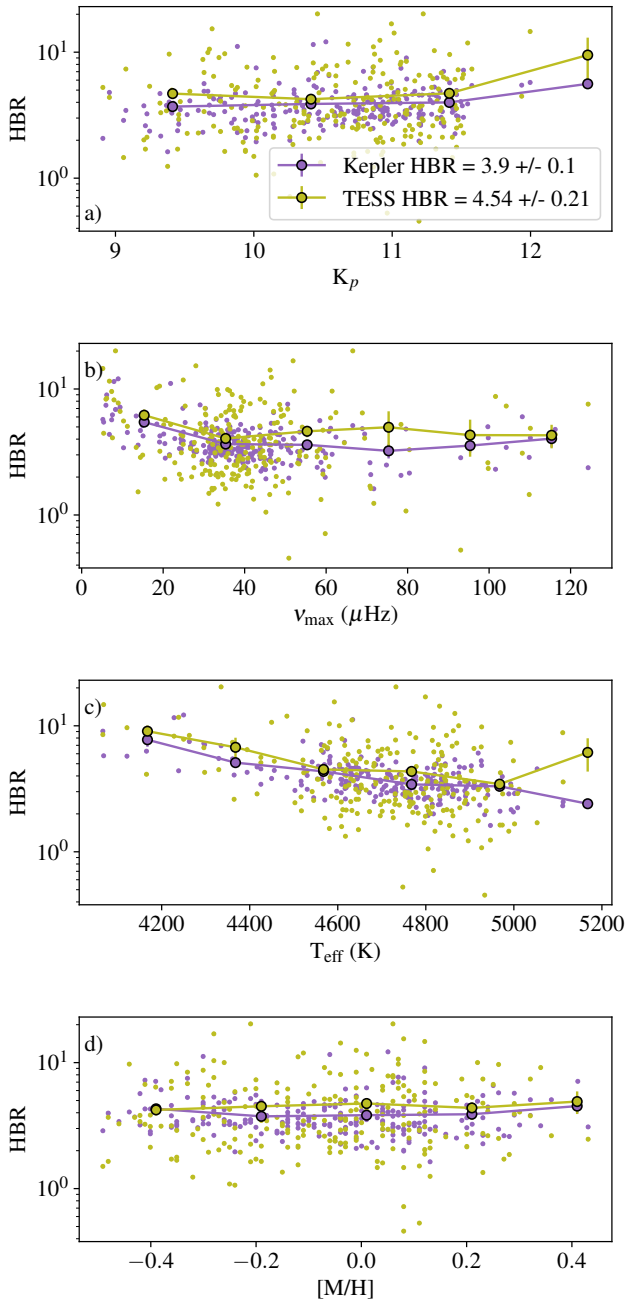

Figure 9. The height-to-background ratio (HBR) from *Kepler* (purple) and TESS (light green) as a function of various parameters. Panel a shows HBR as a function of *Kepler* magnitude, panel b as a function of ν_{max}, panel c as a function of effective temperature and panel d shows it as a function of metallicity.

We next checked how these measured ratios agree with the predicted ratios. Using the effective temperatures and metallicity, we derived the theoretical amplitude ratios using the formalism by Lund (2019). This study found that the amplitude ratios have a slight dependence on effective temperature ($T_{\rm eff}$) and stellar metallicity. Over a range of $T_{\rm eff}$ from 4000 K to 5400 K, the power ratio monotonically decreases from 0.698 to 0.686 as per the black body assumption (solid grey line fig. 8). On the other hand, the predicted values using synthetic stellar spectra increase from 0.58 to 0.68 until 5000 K and starts to decrease for hot temperatures beyond this point (dashed grey line fig. 8). However, both predictions agree in a temperature range from 4200 K and 5800 K. Since the scatter on the observed ratios is larger than this predicted variation, we do not expect this be visible here. It can be seen that the mean value of measured ratio of oscillations follows the theoretical predictions from Lund (2019), for both predictions from using Planck spectrum and using to the stellar model atmospheres. according to Lund (2019). The measured granulation power ratios also agrees with the predictions from using Planck spectrum and synthetic stellar spectrum. Finally, we also checked how these ratios depend upon the evolutionary state and we do not see any significant difference.

3.3 Ratio between oscillation and granulation at $\nu_{\rm max}$

It is important to check how the ratio between oscillation and granulation power in the region of $\nu_{\rm max}$ behaves as a function of wavelength. As this ratio is essentially has a measure of signal-to-noise, it is interesting to check how the HBR behaves at two different wavelengths. Using *Kepler* data spanning 590 days of around 1100 giants, Mosser et al. (2012) have shown that the Oscillation height-to-background ratio (HBR), $\frac{H_{\rm osc}}{B_{\nu_{\rm max}}}$, is constant at all values of $\nu_{\rm max}$, since both $H_{\rm osc}$ and $B_{\nu_{\rm max}}$ have the same dependence on $\nu_{\rm max}$. Kallinger et al. (2014) showed that the variation of granulation amplitude with oscillation is not linear and depends on surface gravity and mass, in *Kepler*.

For the 229 stars with stellar parameters, we used $H_{\rm osc}$ and $B_{\nu_{\rm max}}$ to compute the HBR. Figure 9 shows the variation of HBR over different parameters, for *Kepler* (purple) and TESS (light green). The HBR is lot more constrained in vertical direction for *Kepler* data with a mean HBR of 3.9 ± 0.1. For TESS data, the mean is almost similar (4.54) but has a SEM of ± 0.21. Panel a shows that the HBR is constant over the entire range of *Kepler* magnitude, both for *Kepler* and TESS. The HBR is constant, except at lower $\nu_{\rm max}$ (panel b), possibly due to the difficulty in measuring granulation background at lower frequencies. panel c shows the variation of HBR as a function of $T_{\rm eff}$. We see a slight decrease in HBR as we move to higher temperatures for both *Kepler* and TESS. However, we do not see such an effect when plotted against metallicity, in panel d. In any case, the mean HBR values of TESS don't go below *Kepler* values and hence suggest that the proportion of oscillation and granulation would be preserved in TESS.

4 CONCLUSIONS

In this work, we aimed to study the wavelength dependence of oscillation and granulation powers using light curves from *Kepler* and TESS. Using the publicly available light curves of 282 red giants from *Kepler* and TESS space missions, we arrive at the following conclusions:

- Using the amplitudes of contact binary stars, we find that the method used for light curve extraction and de-trending impacts the amplitudes we measure. Therefore, careful selection of light curves is essential for amplitude studies.

- The observed value of mean ratio of oscillation power in TESS to *Kepler* agrees with theoretical prediction from Lund (2019). Both $\langle P_{\rm osc} \rangle$ and $H_{\rm osc}$ ratios agree with prediction with mean values 0.68 ± 0.01. A global measure of granulation power ($\langle P_{\rm gran} \rangle$) also shows good agreement with predicted ratios. We see

no significant departure to this ratio at any *Kepler* magnitude or time span of TESS-SPOC data.

- Oscillation and granulation have the same wavelength dependence, as predicted by Kjeldsen & Bedding (2011). That is, the granulation signal will attenuate in the same way as oscillation does as we observe through redder wavelengths. This has been shown by the all the cases where the mean oscillation ratio agrees with granulation ratio, in any of the cases considered here.

- The mean oscillation and granulation ratios from observations do not show any significant dependence on effective temperature or metallicity. This shows that observations and corresponding measurements at redder wavelengths do not show any bias towards stars of specific spectral type or class.

- The height-to-background ratio (HBR) of oscillation and granulation at $\nu_{\rm max}$ has a mean value for *Kepler* of 3.9 ± 0.1 and for TESS it is 4.54 ± 0.21. These agree well with each other and with the values determined previously (Mosser et al. 2012; Hekker, S. et al. 2012; Kallinger et al. 2014). This is reassuring for the Roman mission, which will observe at even redder wavelengths, giving no reason to worry that the oscillations might be swamped by granulation.

ACKNOWLEDGEMENTS

KRS would like to acknowledge Mikkel N. Lund and Benjamin Montet for useful discussions on bolometric corrections and light curves. We gratefully acknowledge support from the Australian Research Council through Laureate Fellowship FL220100117, which includes a PhD scholarship for KRS. This work made use of several publicly available `python` packages: `astropy` (Astropy Collaboration 2013, 2018), `lightkurve` (Lightkurve Collaboration et al. 2018), `matplotlib` (Hunter 2007), `numpy` (Harris et al. 2020), and `scipy` (Virtanen et al. 2020). This work has made an extensive use of Topcat (`http://www.star.bristol.ac.uk/~mbt/topcat/`,`Taylor2005`).

DATA AVAILABILITY

The *Kepler* data underlying this article are available at the MAST Portal (Barbara A. Mikulski Archive for Space Telescopes), at `https://mast.stsci.edu/portal/Mashup/Clients/Mast/Portal.html`

REFERENCES

Aerts C., Christensen-Dalsgaard J., Kurtz D. W., 2010, Asteroseismology, doi:10.1007/978-1-4020-5803-5.
Astropy Collaboration 2013, A&A, 558, A33
Astropy Collaboration 2018, AJ, 156, 123
Baglin A., Auvergne M., Barge P., Deleuil M., Catala C., Michel E., Weiss W., COROT Team 2006, in Fridlund M., Baglin A., Lochard J., Conroy L., eds, ESA Special Publication Vol. 1306, The CoRoT Mission Pre-Launch Status - Stellar Seismology and Planet Finding. p. 33
Basu S., Hekker S., 2020, Frontiers in Astronomy and Space Sciences, 7, 44
Benz W., et al., 2021, Experimental Astronomy, 51, 109
Brown T. M., Gilliland R. L., Noyes R. W., Ramsey L. W., 1991, ApJ, 368, 599
Caldwell D. A., et al., 2020, Research Notes of the American Astronomical Society, 4, 201
Chaplin W. J., Miglio A., 2013, ARA&A, 51, 353
Chaplin W. J., et al., 2011, The Astrophysical Journal, 732, 54
Christensen-Dalsgaard J., Frandsen S., 1983, Sol. Phys., 82, 165
Corsaro E., Fröhlich H. E., Bonanno A., Huber D., Bedding T. R., Benomar O., De Ridder J., Stello D., 2013, MNRAS, 430, 2313
Corsaro E., et al., 2017, A&A, 605, A3
Fröhlich C., et al., 1995, Virgo: Experiment for Helioseismology and Solar Irradiance Monitoring. Springer Netherlands, Dordrecht, pp 101–128, doi:10.1007/978-94-009-0191-9_4, `https://doi.org/10.1007/978-94-009-0191-9_4`
Gaia Collaboration et al., 2016, A&A, 595, A1
Gehan C., Campante T. L., Cunha M. S., Pereira F., 2023, Astronomische Nachrichten, 344, e20220090
Goldreich P., Keeley D. A., 1977a, ApJ, 211, 934
Goldreich P., Keeley D. A., 1977b, ApJ, 212, 243
Gould A., Huber D., Penny M., Stello D., 2015, Journal of Korean Astronomical Society, 48, 93
Han T., Brandt T. D., 2023, AJ, 165, 71
Harris C. R., et al., 2020, Nature, 585, 357
Hekker S., Christensen-Dalsgaard J., 2017, A&ARv, 25, 1
Hekker, S. et al., 2012, A&A, 544, A90
Hon M., et al., 2021, The Astrophysical Journal, 919, 131
Houdek G., Dupret M.-A., 2015, Living Reviews in Solar Physics, 12, 8
Huang C. X., et al., 2020a, Research Notes of the American Astronomical Society, 4, 204
Huang C. X., et al., 2020b, Research Notes of the American Astronomical Society, 4, 206
Huber D., 2020, in Monteiro M. J. P. F. G., García R. A., Christensen-Dalsgaard J., McIntosh S. W., eds, Dynamics of the Sun and Stars. Springer International Publishing, Cham, pp 301–312
Huber D., Stello D., Bedding T. R., Chaplin W. J., Arentoft T., Quirion P. O., Kjeldsen H., 2009, Communications in Asteroseismology, 160, 74
Huber D., et al., 2011, The Astrophysical Journal, 743, 143
Hunter J. D., 2007, Computing in Science & Engineering, 9, 90
Jackiewicz J., 2021, Frontiers in Astronomy and Space Sciences, 7
Jenkins J. M., et al., 2010, ApJ, 713, L120
Jenkins J. M., et al., 2016, in Chiozzi G., Guzman J. C., eds, Society of Photo-Optical Instrumentation Engineers (SPIE) Conference Series Vol. 9913, Software and Cyberinfrastructure for Astronomy IV. p. 99133E, doi:10.1117/12.2233418
Kallinger T., et al., 2014, A&A, 570, A41
Karoff C., et al., 2013, The Astrophysical Journal, 767, 34
Kjeldsen H., Bedding T. R., 1995, A&A, 293, 87
Kjeldsen H., Bedding T. R., 2011, A&A, 529, L8
Kjeldsen H., et al., 2005, ApJ, 635, 1281
Lightkurve Collaboration et al., 2018, Lightkurve: Kepler and TESS time series analysis in Python, Astrophysics Source Code Library (ascl:1812.013)
Lomb N. R., 1976, Ap&SS, 39, 447
Ludwig H. G., et al., 2009, A&A, 506, 167
Lund M. N., 2019, MNRAS, 489, 1072
Mathur S., et al., 2011, ApJ, 741, 119
Mosser B., et al., 2012, A&A, 537, A30
Murray N., 1993, in Brown T. M., ed., Astronomical Society of the Pacific Conference Series Vol. 42, GONG 1992. Seismic Investigation of the Sun and Stars. p. 3
Penny M. T., Gaudi B. S., Kerins E., Rattenbury N. J., Mao S., Robin A. C., Calchi Novati S., 2019, ApJS, 241, 3
Pepe F., et al., 2013, The Messenger, 153, 6
Press W. H., Rybicki G. B., 1989, ApJ, 338, 277
Prša A., et al., 2011, AJ, 141, 83
Ricker G. R., et al., 2014, in Oschmann Jacobus M. J., Clampin M., Fazio G. G., MacEwen H. A., eds, Society of Photo-Optical Instrumentation Engineers (SPIE) Conference Series Vol. 9143, Space Telescopes and Instrumentation 2014: Optical, Infrared, and Millimeter Wave. p. 914320 (`arXiv:1406.0151`), doi:10.1117/12.2063489

Rodríguez Díaz L. F., Bigot L., Aguirre Børsen-Koch V., Lund M. N., Rørsted J. L., Kallinger T., Sulis S., Mary D., 2022, MNRAS, 514, 1741
Samadi R., Belkacem K., Dupret M. A., Ludwig H. G., Baudin F., Caffau E., Goupil M. J., Barban C., 2012, A&A, 543, A120
Samadi R., Belkacem K., Sonoi T., 2015, in EAS Publications Series. pp 111–191 (arXiv:1510.01151), doi:10.1051/eas/1573003
Scargle J. D., 1982, ApJ, 263, 835
Smith J. C., et al., 2012, PASP, 124, 1000
Sreenivas K. R., Bedding T. R., Li Y., Huber D., Crawford C. L., Stello D., Yu J., 2024, MNRAS, 530, 3477
Stello D., et al., 2011, ApJ, 737, L10
Stello D., et al., 2022, MNRAS, 512, 1677
Stumpe M. C., et al., 2012, PASP, 124, 985
Sulis, S. Lendl, M. Hofmeister, S. Veronig, A. Fossati, L. Cubillos, P. Van Grootel, V. 2020, A&A, 636, A70
Sulis, S. et al., 2023, A&A, 670, A24
Tassoul M., 1980, Astrophysical Journal Supplement Series, vol. 43, Aug. 1980, p. 469-490., 43, 469
Trampedach R., Christensen-Dalsgaard J., Nordlund A., Stein R. F., 1998, in Kjeldsen H., Bedding T. R., eds, The First MONS Workshop: Science with a Small Space Telescope. p. 59
Van Cleve J. E., Caldwell D. A., 2016, Kepler Instrument Handbook, Kepler Science Document KSCI-19033-002, id.1. Edited by Michael R. Haas and Steve B. Howell
Virtanen P., et al., 2020, Nature Methods, 17, 261
Vrard M., Kallinger T., Mosser B., Barban C., Baudin F., Belkacem K., Cunha M. S., 2018, A&A, 616, A94
Yu J., Huber D., Bedding T. R., Stello D., Hon M., Murphy S. J., Khanna S., 2018, ApJS, 236, 42
Yu J., Khanna S., Themessl N., Hekker S., Dréau G., Gizon L., Bi S., 2023, The Astrophysical Journal Supplement Series, 264, 41
Zhou Y., Asplund M., Collet R., Joyce M., 2020, MNRAS, 495, 4904

This paper has been typeset from a TEX/LATEX file prepared by the author.